Proceedings of the 12th International Conference on Fluid Flow, Heat and Mass Transfer (FFHMT 2025)
July 15, 2025 - July 17, 2025 | Imperial College London Conference, London, United Kingdom
Paper No. 119
DOI: 10.11159/ffhmt25.119

A Study of Slurry Flow in Annular Jet Pump for Optimized Specific Energy Consumption—A Mixture Model Approach

Sadia Riaz, Jussi Aaltonen, and Kari Koskinen
Mechatronics Research Group (MRG), Unit of Automation Technology and Mechanical Engineering,
Faculty of Engineering and Natural Sciences, Tampere University, Korkeakoulunkatu 7, 33720 Tampere, Finland.
sadia.riaz@tuni.fi; jussi.aaltonen@tuni.fi; kari.koskinen@tuni.fi
Corresponding author email: sadia.riaz@tuni.fi

Abstract – Efficient mining operations rely on effectively transporting slurry and minerals, directly impacting cost, productivity, and sustainability. Annular Jet Pumps (AJPs) offer a robust solution due to their simple design, absence of moving parts, and minimal maintenance requirements. This study investigates the flow behavior of a sand-water slurry through an AJP, focusing on optimizing Specific Energy Consumption (SEC) to promote energy-efficient mining. A CFD approach, i.e., the mixture model, this analysis captures intricate interactions between solid particles and the carrier fluid, and the Realizable k-ε turbulence model complements the mixture model to visualize key turbulence parameters. A parametric study explores the effects of sand particle size, volume fraction, and geometric parameters (such as nozzle radius and convergence angle on slurry suction and pressure distribution). Findings reveal that optimizing these parameters significantly enhances suction capacity while reducing SEC, reinforcing the energy efficiency of AJPs for mining applications. Validation against established literature, including experimental and numerical studies, demonstrates excellent agreement, confirming the model's accuracy in predicting slurry flow behavior. This work highlights the potential of AJPs as sustainable and efficient solutions for mining, ensuring reduced energy consumption, minimal resource wastage, and enhanced system performance.

Keywords**:** Slurry transport, mixture model, realizable k-ε turbulence model, Specific Energy Consumption (SEC), Annular Jet Pump (AJP), particle size, volume fraction.

1. Introduction

Due to the complex interactions between solid particles and the carrier fluid, efficient sand-water slurry transport is crucial in industries like mining, dredging, and petroleum. Annular Jet Pumps (AJPs) are favored for transporting multiphase mixtures without mechanical parts, reducing maintenance costs. However, optimizing AJPs for slurry transport requires understanding parameters like particle size, concentration, rheology, and geometrical features (e.g., throat dimensions, nozzle angles). Key flow characteristics, including velocity profiles, pressure distribution, and phase mixing efficiency, are vital for reliable performance. (1).

CFD models, including Eulerian-Lagrangian, Eulerian-Eulerian, and mixture models, are essential for studying slurry flows. The Eulerian-Lagrangian model offers detailed particle-scale insights but is computationally intensive for high particle concentrations. The Eulerian-Eulerian model handles dense flows efficiently but lacks particle-level detail. The mixture model balances the slurry as a single continuum with averaged properties, which is ideal for well-mixed phases and less critical particle-fluid interactions. (2). Extensive research has been conducted on slurry transport systems, including their integration into jet pumps. Jet pumps are broadly classified into Centre Jet Pumps (CJPs) and Annular Jet Pumps (AJPs), with literature indicating that AJPs offer higher efficiency. However, significant opportunities remain to enhance the design and performance of AJPs.

Shimizu (3) demonstrated that AJPs can achieve efficiencies up to 36%, comparable to Central Jet Pumps, and highlighted the impact of swirl on performance. Kökpinar & Gögus (4) optimized water jet pumps for slurry transport, achieving 33% efficiency and introducing a bypass system to reduce wear on centrifugal pumps. Xinping Long and his team at Wuhan University have extensively studied slurry transport through AJPs over the past two decades. They investigated cavitation initiation and development under varying flow rate ratios and optimized AJP design using Design of Experiments (DOE), CFD, and experiments. They analyzed cavitation in jet pumps with different area ratios. They employed Large Eddy Simulations (LES) to study flow characteristics and turbulent coherent structures (5), revealing vortex behavior in recirculation regions and boundary layers. Later, they examined cavity-length pulsation characteristics in jet pumps (6) and

cavitation behavior under negative flow ratios (7), providing insights into pressure ratio effects on cavitation areas and enhancing AJP design and performance understanding.

Singh et al. (8) employed CFD to study slurry flow, comparing their two-phase mixture model, incorporating algebraic slip and turbulent dispersion, with the models proposed by Kaushal et al. (9), in 2012. Their model demonstrated accurate pressure drop predictions, challenging earlier results despite variations in solids concentration profiles. They emphasized the model's simplicity and suitability for engineering applications, highlighting its potential for pressure drop prediction. They also called for further research to enhance solids concentration profile accuracy in slurry flow pipelines.

Messa (2) conducted a comprehensive review of CFD methods for slurry transport, including the Eulerian-Eulerian, Eulerian-Lagrangian, and Mixture models, emphasizing the mixture model's versatility across diverse solid volume fractions. Over the past decade, Messa and Matoušek (10),(11) advanced research on pipeline slurry transport using CFD and experiments. They employed the β-σ two-fluid model (12) , an extension of the Eulerian approach to study horizontal pipe flows under various conditions, such as differing solid sizes and slurry types. Kai et al. (13) studied multi-nozzle AJPs using CFD simulations, focusing on nozzle geometry and pump performance. Their work, validated experimentally, also optimized AJPs using the Kriging model (14) with CFD and experimental data. Wang et al. (15) introduced the Streamlined Annular Jet Pump (SAJP) to improve flow smoothness and minimize energy loss in the Early Annular Jet Pump (EAJP), using the realizable k-epsilon and Schnerr-Sauer cavitation models in separate simulations for both pump types.

This study employs a multiphase mixture model to simulate the complex interactions between solid particles and the carrier fluid within an AJP. The objective is to develop a robust and efficient AJP design tailored for sand and water slurry transport, addressing challenges posed by multiphase flow dynamics and providing practical solutions for industrial applications, particularly in mining and mineral processing. In this research, a mixture model (16) with realizable k-ε is employed to study the slurry flow in AJP to optimize its SEC. A detailed parametric study shows the effect of the primary fluid`s volumetric flow, convergence angle, throat diameter, secondary flow inlet diameter, sand particle size, and volume fraction. These parameters can improve the suction pressure of the AJP, and consequently, the SEC will be reduced, which is the focus of this paper.

Sadia et al. (17) recently examined the structural factors influencing suction performance in AJPs, focusing on the primary fluid's flow rate, convergence angle, and throat diameter. Numerical simulations using the Realizable k-ε turbulence model were validated experimentally, showing strong agreement with a mean absolute error (MAE) of 1.71 kPa and a root mean square error (RMSE) of 2.02 kPa. Optimizing the convergence angle (27°) and throat diameter (10 mm) enhanced suction capacity at a flow rate of 10 m^3/h, achieving 34% efficiency at flow ratios of 0.4 to 0.6. These results confirm the model's reliability and the AJP's suitability for energy-efficient industrial applications. They also studied Specific energy consumption optimization for AJP using mixture model. Same researcher (18) studied AJP geometric design for slurry transport major and testing of the full-scale prototype has been executed in an opencast oil-shale mine under (partly) submerged conditions. During the field tests, the working principle of the Venturi ore transport system could be proven by successful transport of excavated oil-shale up to a certain grain size. In a related study, Berners et al. (18) explored the optimization of specific energy consumption in AJPs using the Mixture Model. Additionally, they examined the geometric design of AJPs for slurry transport and conducted full-scale prototype testing in an opencast oil-shale mine under partially submerged conditions. Field tests successfully demonstrated the working principle of the Venturi-based ore transport system, effectively transporting excavated oil shale up to a certain grain size, confirming the practical feasibility of the AJP system in real-world mining applications.

As this study is a step towards efficient mining, the reduced energy consumption plays a crucial role in utilizing AJP in mineral extraction. This work is compared with research by (14) for the AJP modeling. The results are also benchmarked against the numerical analysis of Singh et al. (8), as well as the combined numerical simulations and experimental investigations carried out by Kaushal (9). The validation of the results demonstrates that this model is highly suitable for simulating slurry flow through AJPs, as it balances computational efficiency and accuracy, making it a preferred choice for practical applications. The existing literature primarily uses efficiency as the sole metric for

evaluating system effectiveness. However, this article expands on this by conducting a parametric study on design variables and presenting results for reduced SEC. This metric has not been previously addressed in the literature.

2. Mathematical Model

An AJP consists of three key components: the converging section, the diverging section, and the throat. In the converging section, the primary fluid (water) creates an annulus, generating a vacuum at the throat to suction the secondary fluid (slurry). The AJP in this study is modular, allowing for interchangeable nozzle designs with a single core, as shown in Figure 1 (17). Pressure is measured at four critical points: the primary and secondary fluid inlets, the throat, and the diffuser. Key geometric parameters, such as throat length, diameter, and convergence angle, are critical for pump efficiency, affecting mixing, friction, and vacuum generation. The volumetric flow rate of the primary fluid also influences slurry suction. The AJP is 3D printed for physical testing, supporting material optimization by fabricating only the nozzle for different designs.

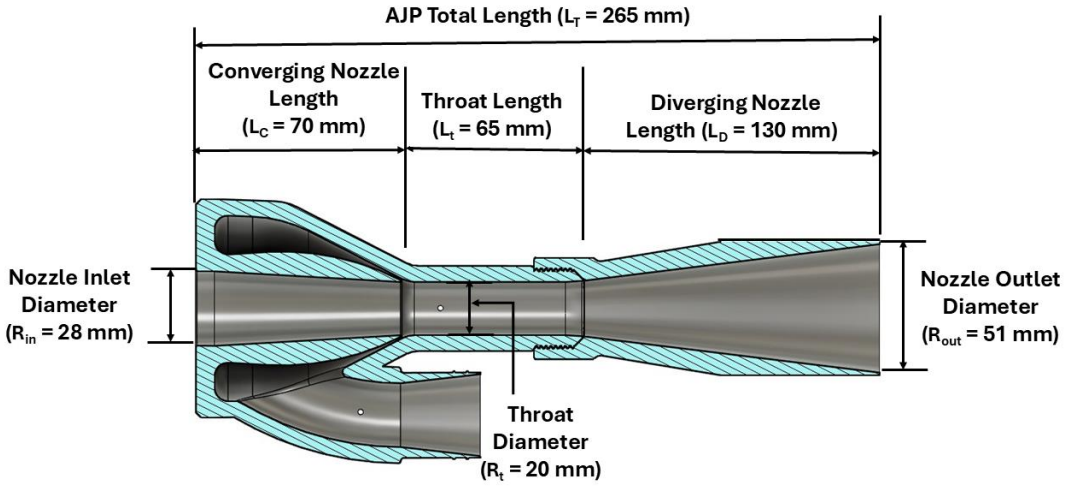

Figure 1: Cut section of the proposed Venturi pump design showing different sections along the flow direction.

The Mixture model is employed to simulate the flow within the internal flow field of AJP, ensuring compliance with the hydrodynamic equations, primarily the continuity and momentum conservation equations. The pressure distribution is calculated from a mixture averaged continuity equation, and the velocity of the dispersed phase is described using a slip model. The volume fraction of the dispersed phase is tracked by solving a transport equation for the volume fraction. Turbulence effects are modeled using the realizable two-equation k-ε model. Flow close to walls is modeled using wall functions.

Table 1: Mixture model equations (16)

$\rho = \emptyset_c \rho_c + \emptyset_d \rho_d$	(1)
$\rho_t + \nabla \cdot (\rho \mathbf{u}) = 0$	(2)
$\nabla \cdot \mathbf{j} = m_{dc}\left(\frac{1}{\rho_c} - \frac{1}{\rho_d}\right)$	(3)
$\rho \mathbf{j}_t + \rho(\mathbf{j} \cdot \nabla) + \rho_c \varepsilon\left(\mathbf{j}_{\text{slip}} \cdot \nabla\right)\mathbf{j} = -\nabla p + \nabla \cdot \tau_{\text{Gm}} + \rho \text{g} + \boldsymbol{F} - \nabla \cdot \left[\rho_c (1 + \emptyset_c \varepsilon)\mathbf{u}_{\text{slip}} \mathbf{j}_{\text{slip}}{}^{\text{T}}\right] - \rho_c \varepsilon \left[(\mathbf{j} \cdot \nabla)\mathbf{j}_{\text{slip}} + \left(\nabla \cdot (\text{D}_{\text{md}} \nabla \emptyset_{\text{d}})\right)\mathbf{j} + \mathbf{j}_{\text{slip}} \text{m}_{\text{dc}} \left(\frac{1}{\rho_c} - \frac{1}{\rho_d}\right)\right]$	(4)

$\mathbf{j}_{\text{slip}} = \emptyset_{\text{d}}\rho_{\text{c}}\mathbf{u}_{\text{slip}}$	(5)
$\frac{3}{4}\frac{C_d}{d_d}\lvert\mathbf{u}_{\text{slip}}\rvert\mathbf{u}_{\text{slip}} = -\frac{(\rho-\rho_d)}{\rho_c}\left(-\mathbf{j}_t - (\mathbf{j}\cdot\nabla)\mathbf{j} + \mathbf{g} + \frac{\mathbf{F}}{\rho}\right)$	(6)
$\rho\frac{\partial k}{\partial t} = +\rho\mathbf{u}\cdot\nabla k = \nabla\cdot\left(\left(\mu + \frac{\mu_T}{\sigma_k}\right)\nabla k\right) + P_k - \rho\varepsilon$	(7)
$P_k = \mu_T\left(\nabla\mathbf{u}\colon(\nabla\mathbf{u} + (\nabla\mathbf{u})^{\boldsymbol{T}}) - \frac{2}{3}(\nabla\cdot\mathbf{u})^2\right) - \frac{2}{3}\rho k\nabla\cdot\mathbf{u}$	(8)
$\rho\frac{\partial\varepsilon}{\partial t} + \rho\mathbf{u}\cdot\nabla\varepsilon = \nabla\cdot\left(\left(\mu + \frac{\mu_T}{\sigma_\varepsilon}\right)\nabla\varepsilon\right) + C_1\rho S\varepsilon - C_{\varepsilon 2}\rho\frac{\varepsilon^2}{k+\sqrt{\nu\varepsilon}}$	(9)

The mixture density is given in equation (1), where $\emptyset_c$ and $\emptyset_d$ denote the volume fractions of the continuous phase and the dispersed phase, respectively, ρ_c is the continuous phase density (SI unit: kg/m^3), and ρ_d is the dispersed phase density (SI unit: kg/m^3). In the Mixture Model interfaces it is assumed that the densities of both phases, ρ_c and ρ_d, are constant. Therefore, equation (3) is the alternative form of the continuity equation for the mixture. Equation (4) is the momentum equation for the mixture where **j** is the velocity vector (SI unit: m/s), ρ is the density (SI unit: kg/m^3), p is the pressure (SI unit: Pa), ε is the reduced density difference (SI unit: kg/kg), D_{md} is a turbulent dispersion coefficient (SI unit: m^2/s), m_{dc} is the mass transfer rate from the dispersed to the continuous phase (SI unit: kg/(m^3·s)), g is the gravity vector (SI unit: m/s^2), and F is any additional volume force (SI unit: N/m3).$\mathbf{u}_{\text{slip}}$ is the slip velocity vector between the two phases (SI unit: m/s),$\mathbf{j}_{\text{slip}}$ is the slip flux (SI unit: m/s), τ_{Gm} is the sum of the viscous and turbulent stresses (SI unit: kg/(m·s^2)). The slip flux is defined for in equation (5) where, $\mathbf{u}_{\text{slip}}$ (m/s) denotes the relative velocity between the two phases. For more details of the model (19) is referred. The Schiller-Naumann model is used for the relative velocity between the two phases, $\mathbf{u}_{\text{slip}}$ which uses the relationship for the slip velocity as shown in equation (6), where C_d (dimensionless) is the particle drag coefficient (20). Essentially, the relation is interpreted as a balance between viscous drag and buoyancy forces acting on the dispersed phase. For the turbulence modeling, the realizable k- ε model is used. The realizable k-ε turbulence model is an extension of the standard k-ε model. Compared to the standard k-ε model, the realizable k-ε model yields better predictions for specific flows. One example is the round jet, for which the standard k-ε model overestimates the spreading rate. Since the realizability conditions are approached asymptotically, the turbulence characteristics are more consistent than the standard k-ε model. The realizable k-ε model introduces two additional transport equations and two dependent variables: the turbulent kinetic energy, k, and the turbulent dissipation rate, ε. The transport equation for the turbulent kinetic energy is the same as for the standard k-ε model where the production term is shown in equation (8). Equation (9) shows the transport equation for the turbulent dissipation rate. As the details of the model are available in books and online tutorials, readers are referred to references. (19) and (20).

3. Results and Analysis

This section demonstrates the result and analysis section for the proposed mixture model coupled with realizable k-ε turbulence model. Figure 2 validates the model developed in this study by comparing the predicted pressure drop per unit length (kPa/m) with inlet bulk velocity (Vin in m/s) against benchmark data from previous literature, including Kaushal's experimental and numerical models (2012) and Singh's numerical model (2023). Kaushal's experimental data (blue line) demonstrates a linear increase in pressure drop with inlet velocity, attributed to heightened viscous and inertial effects. The orange line, representing Kaushal's mixture model, slightly overpredicts the pressure drops, indicating an overestimation of

particle-fluid interaction resistance. Kaushal's Eulerian model (grey line) aligns well with experimental results at lower velocities but diverges at higher velocities, revealing limitations in capturing turbulence at elevated flow rates. Singh's model (yellow line) closely follows Kaushal's experimental and mixture model trends, affirming its reliability in predicting slurry flow behavior. The current study's model (dark blue line) exhibits excellent agreement with Kaushal's experimental data and Singh's model across the entire velocity range. This consistency validates the accuracy and robustness of the model in capturing key physical phenomena, including turbulence, particle-fluid interactions, and wall shear effects. These results confirm the reliability of the proposed model as a valuable tool for designing and optimizing Annular Jet Pump systems for efficient slurry transport.

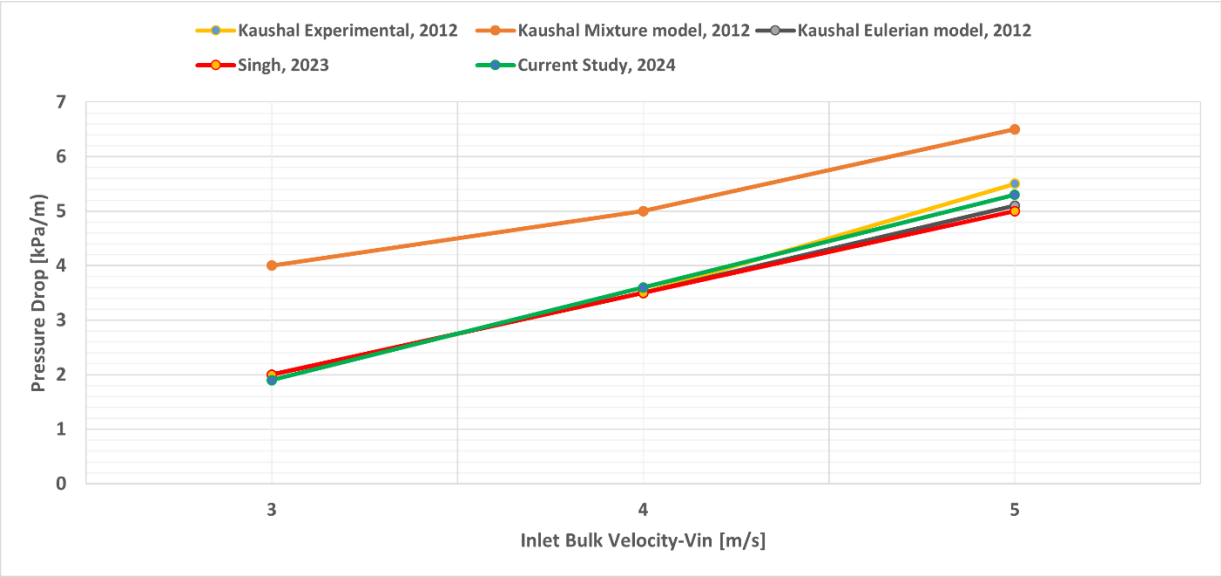

Figure 2: Comparison of pressure drop predictions from this study to the results of the mixture model of Singh et al. (2023), the mixture model, the granular model, and experimental data of Kaushal et al. (2012) at 30% sand concentration in slurry

This section presents the result and analysis of the mixture model for the slurry flow in AJP. Here, water is the primary fluid, which provides the volumetric flow rate (Q) for the suction of slurry (sand and water), which is the secondary fluid. Table 2 shows the simulation parameters that are used to conduct this simulation:

Table 2: Simulation parameter

Simulation Parameter	**Value**
Maximum Flow Capacity (Q)	10 m^3/h
Throat radius of nozzle (r_T)	10 mm
Inlet radius of nozzle (r_I)	14 mm
Outlet radius of nozzle (r_O)	25.5 mm
Convergence angle of nozzle (α)	27°
Divergence radius of nozzle (β)	7°
Length of nozzle throat (L_T)	65 mm
AJPs total length	300 mm

Density of continuous phase (water)	1000 kg/m^3
Density of dispersed phase (sand)	2600 kg/m^3
Viscosity of continuous phase (water)	0.001 Pa·s
The dispersed phase volume fraction	0.2
Maximum packing concentration	0.62
Average concentration	0.35
Particle diameter (Dp)	0.3 mm

Figure 3 provides a comprehensive analysis of the pressure distribution along the axial length of an AJP using a 1D pressure graph and a 3D contour plot. The 1D graph illustrates a sharp pressure drop from the inlet, reaching a minimum at the throat and gradually recovering towards the outlet. This behavior, characteristic of jet pumps, results from fluid acceleration in the nozzle (causing low pressure) and deceleration in the diffuser (facilitating pressure recovery). The 3D contour plot complements this by visualizing the spatial pressure distribution, with the throat exhibiting the lowest pressure zones essential for entraining the secondary slurry flow. The gradual pressure recovery downstream ensures proper discharge dynamics. These insights are crucial for optimizing AJP design for efficient slurry transport.

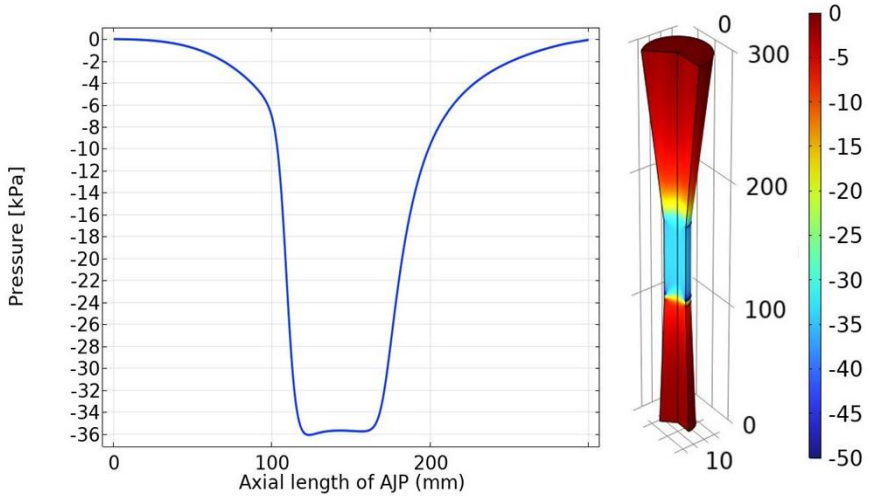

Figure 3: Pressure distribution along axial length of AJP

The parametric study of the AJP shown in figure 4 highlights the flow rate, convergence angle, sand volume fraction, and particle size effects on axial pressure distribution. As shown in Figure 4(a), increasing the flow rate causes a more significant pressure drop at the throat due to the Venturi effect, with partial recovery in the diffuser. Figure 4(b) illustrates that larger convergence angles amplify the pressure drop at the throat and enhance recovery efficiency through stronger fluid acceleration and deceleration. In Figure 4(c), higher sand volume fractions lead to more significant pressure drops and reduced recovery efficiency due to increased drag forces and turbulence, disrupting flow stabilization. Lastly, Figure 4(d) demonstrates that bigger particle size tends to increase the pressure distribution on axial length of AJP, emphasizing that the AJP's geometry and operating conditions primarily dictate performance. These findings showcase the AJP's robustness and adaptability under varying conditions and slurry compositions.

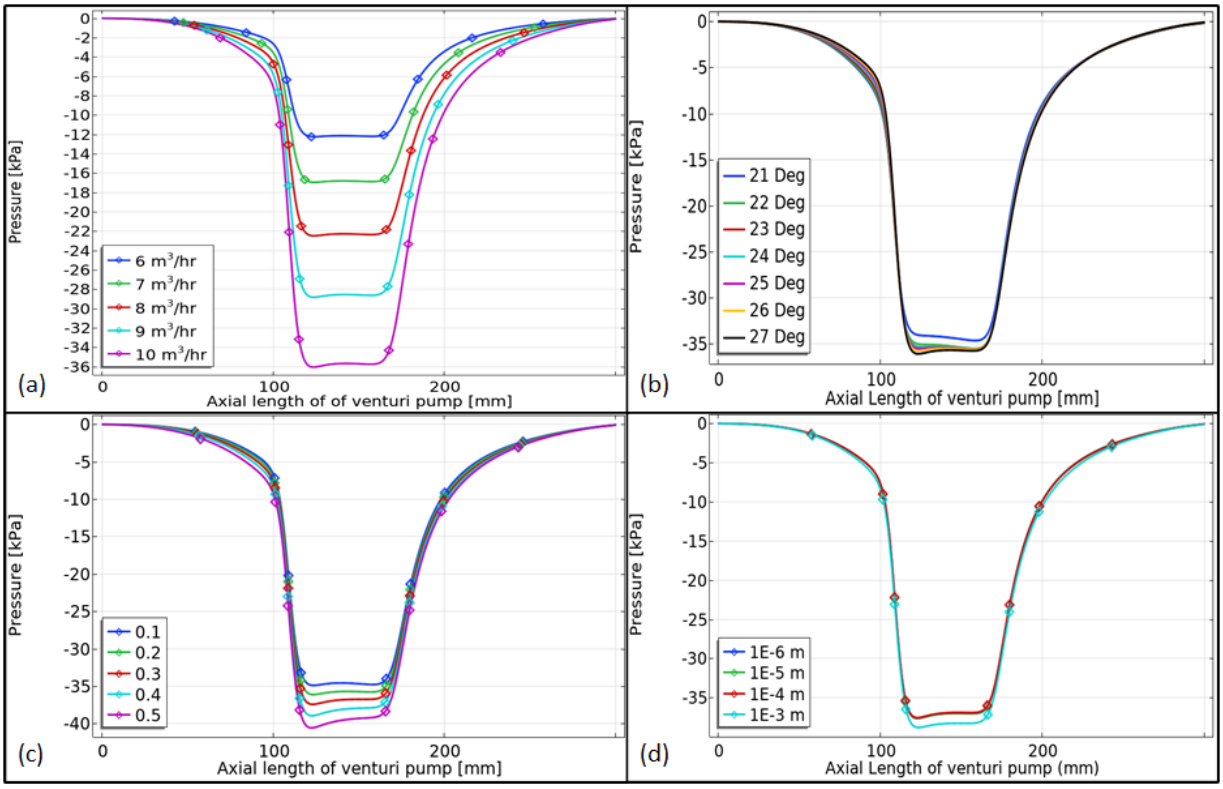

Figure 4: (a) Pressure variation at different volumetric flow rates of primary fluid, (b) Variation of pressure along the axial length of AJP at different nozzle convergence angles, (c) Pressure distribution along the axial length of AJP at different volume fractions of sand particles, (d) Pressure distribution along the axial length of AJP at different sand particle sizes

Figure 5 analyses the variation in SEC for an AJP handling a sand-water slurry influenced by operational and geometric parameters. In Figure 5(a), SEC increases with the primary fluid's volumetric flow rate (Q), reflecting higher energy demands due to enhanced viscous losses and momentum exchange. Figure 5(b) shows that SEC decreases with smaller convergence angles (α) due to efficient mixing but rises sharply beyond an optimal angle due to turbulence and flow separation. In Figure 5(c), SEC increases as the suction nozzle radius (R_{in}) grows, driven by greater entrained slurry volume, enhanced turbulence, and drag forces. Figure 5(d) highlights a decrease in SEC with increasing sand volume fraction (VF) from 0.1 to 0.5, attributed to improved energy transfer efficiency, though excessive concentrations could pose challenges. Finally, Figure 5(e) demonstrates a steady rise in SEC with increasing sand particle size (Dp), linked to greater drag forces and flow

resistance. These results emphasize the interplay of pump design, operational conditions, and slurry properties in optimizing energy efficiency.

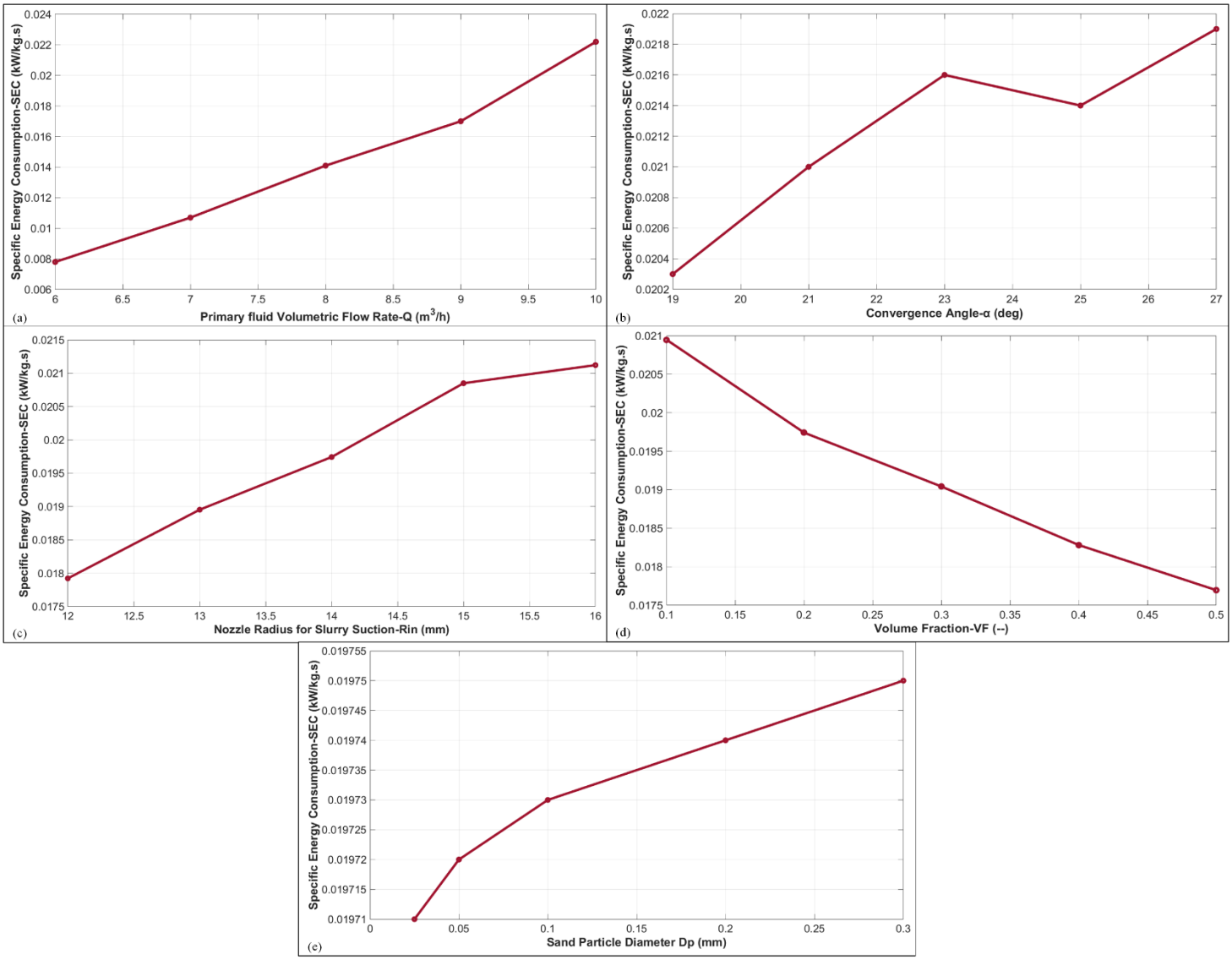

Figure 5: (a) SEC against primary fluid volumetric flow rate, (b) SEC against convergence angle, (c) SEC against slurry inlet radius, (d) SEC against sand volume fraction, and (e) SEC against sand particle diameter

4. Conclusion

This study demonstrates the effectiveness of AJPs in optimizing the transport of sand-water slurry, a critical component in efficient and sustainable mining operations. The complex interactions between solid particles and carrier fluid were analyzed using a CFD approach (a mixture model with the realizable k-ε turbulence model) to optimize SEC. The parametric study highlighted the impact of key factors, such as sand particle size, volume fraction, and geometric parameters, on the pump's suction capacity and pressure distribution. Results showed that optimizing these parameters

significantly enhances pump efficiency and reduces Specific Energy Consumption. Validation against established literature, including experimental and numerical studies, confirmed the model's accuracy in predicting slurry flow behavior. The findings demonstrated strong agreement with prior work, further establishing the robustness of the proposed model. By addressing previously unexplored aspects, such as SEC reduction, this research contributes to designing and operating AJPs as energy-efficient and cost-effective solutions for mining and mineral processing. The insights gained from this work underscore the critical role of design optimization in maximizing AJP performance, emphasizing its potential to support sustainable mining practices through reduced energy consumption and enhanced operational efficiency. Future studies could extend this approach to explore additional multiphase flow scenarios and more complex geometries, further advancing the application of AJPs in industrial slurry transport systems.

Acknowledgments

This project has received funding from the European Union's Horizon 2020 research and innovation program under grant agreement 820971.

References

1. Elger D F, Taylor Sam J, Liou C P. Recirculation in an Annular-Type Jet Pump. J Fluids Eng. 1994;735–40.
2. Messa GV, Yang Q, Adedeji OE, Chára Z, Duarte CAR, Matoušek V, et al. Computational fluid dynamics modelling of liquid–solid slurry flows in pipelines: State-of-the-art and future perspectives. Processes. 2021 Sep 1;9(9).
3. Nakamura S, Kuzuhara S, Teacher SK. Yukimaru Shimizu Studies of the Configuration and Performance of Annular Type Jet Pumps [Internet]. 1987. Available from: http://asmedigitalcollection.asme.org/fluidsengineering/article-pdf/109/3/205/5751567/205_1.pdf
4. Kökpinar MA, Göğüş M. THE PERFORMANCE OF WATER JET PUMPS AND THEIR APPLICATION IN SLURRY TRANSPORTATION. Isi Bilimi Ve Teknigi Dergisi/ Journal of Thermal Science and Technology. 2023;43(1):119–34.
5. Xu M Sen, Yang XL, Long XP, Lyu Q, Ji B. Numerical investigation of turbulent flow coherent structures in annular jet pumps using the LES method. Sci China Technol Sci. 2018 Jan 1;61(1):86–97.
6. Wang J, Xu S, Cheng H, Ji B, Zhang J, Long X. Experimental investigation of cavity length pulsation characteristics of jet pumps during limited operation stage. Energy. 2018 Nov 15;163:61–73.
7. Long X, Wang J, Zhang J, Ji B. Experimental investigation of the cavitation characteristics of jet pump cavitation reactors with special emphasis on negative flow ratios. Exp Therm Fluid Sci. 2018 Sep 1;96:33–42.
8. Singh J, Catsoulis S, Lakehal D, Narayanan C. Predicting pressure-drop for pseudo-homogeneous slurry flows using the mixture model at high solids concentrations. International Journal of Multiphase Flow. 2023 Feb 1;159.
9. Kaushal DR, Thinglas T, Tomita Y, Kuchii S, Tsukamoto H. CFD modeling for pipeline flow of fine particles at high concentration. International Journal of Multiphase Flow. 2012 Jul;43:85–100.
10. Messa GV, Matoušek V. Analysis and discussion of two fluid modelling of pipe flow of fully suspended slurry. Powder Technol. 2020 Jan 15;360:747–68.
11. Messa GV, Yang Q, Rasteiro MG, Faia P, Matoušek V, Silva RC, et al. Computational Fluid Dynamic Modelling of Fully-Suspended Slurry Flows in Horizontal Pipes with Different Solids Concentrations. KONA Powder and Particle Journal. 2023;2023(40):219–35.
12. Messa G V., Malin M, Matoušek V. Parametric study of the β - σ two-fluid model for simulating fully suspended slurry flow: effect of flow conditions. Meccanica. 2021 May 1;56(5):1047–77.
13. Xu K, Wang G, Wang L, Yun F, Sun W, Wang X, et al. CFD-Based study of nozzle section geometry effects on the performance of an annular multi-nozzle jet pump. Processes. 2020 Feb 1;8(2).
14. Xu K, Wang G, Wang L, Yun F, Sun W, Wang X, et al. Parameter analysis and optimization of annular jet pump based on Kriging model. Applied Sciences (Switzerland) [Internet]. 2020 Nov 1 [cited 2024 Jan 23];10(21):1–16. Available from: https://www.mdpi.com/2076-3417/10/21/7860#
15. Wang X, Chen Y, Li M, Xu Y, Wang B, Dang X. Numerical study on the working performance of a streamlined annular jet pump. Energies (Basel). 2020 Sep 1;13(17).

16. Manninen Mikko, Taivassalo Veikko, Kallio Sirpa. On the mixture model for multiphase flow. Technical Research Centre of Finland; 1996.
17. Riaz S, Aaltonen J, Pinkse T, Koskinen K. Parametric study of structural influences on suction performance in an Annular Jet Pump—CFD and experimental validation. Journal of Water Process Engineering [Internet]. 2025 Feb;70:107066. Available from: https://linkinghub.elsevier.com/retrieve/pii/S2214714425001382
18. Berner M, Pinkse T, Riaz S, Aaltonen J, Koskinen K. Slurry Transport System of the ROBOMINERS Prototype. Event title11 Kolloquium "Fördertechnik im Bergbau" 2024. 2024 Feb;11(1):26.
19. Comsol. The CFD Module User's Guide [Internet]. 2020. Available from: www.comsol.com/blogs
20. Crowe CT. Multiphase flows with droplets and particles. CRC Press; 2012. 494 p.